CMS Physics Analysis Summary

Contact: cms-pag-conveners-susy@cern.ch 2016/08/04

Search for electroweak production of charginos and neutralinos in the WH final state at 13 TeV

The CMS Collaboration

Abstract

A search is performed for beyond the standard model physics in events with a leptonically-decaying W boson, a Higgs boson decaying to a pair of b-quarks, and missing transverse energy, using 12.9 fb^{-1} of data recorded by CMS in 2016 at $\sqrt{s} = 13$ TeV. This signature is predicted to occur, for example, in supersymmetric models from electroweak production of gauginos. The observed data are in agreement with the standard model prediction. The results are used to set cross section limits on chargino-neutralino production in a simplified model of supersymmetry with the decays $\tilde{\chi}_1^{\pm} \to W\tilde{\chi}_1^0$ and $\tilde{\chi}_2^0 \to H\tilde{\chi}_1^0$.

1 Introduction

Supersymmetry (SUSY) [1–8] is an attractive extension to the standard model (SM), which is based on a new symmetry between bosons and fermions. It predicts the existence of a superpartner for every SM particle, with the same quantum numbers but differing by one half unit of spin. In R-parity conserving SUSY models, supersymmetric particles are created in pairs, and the lightest supersymmetric particle (LSP) is stable [9, 10]. As a result, SUSY also provides a potential connection to cosmology as the LSP, if neutral and stable, may be a viable dark matter candidate.

Early searches using 13 TeV Large Hadron Collider data focused on strong production of SUSY particles, such as squarks and gluinos. Pair production of these particles is predicted by theory to have the largest cross-section and therefore offers quick discovery potential. Typical searches for squarks and gluinos require significant hadronic activity in events, manifesting itself in a large number of energetic jets. However, the absence of observed signal in these searches suggests that strongly produced SUSY particles may be too massive to be probed with the current datasets. In contrast, neutralinos (χ^0) and charginos ($\chi^\pm$), mixtures of the superpartners of the SM electroweak gauge bosons and the Higgs boson, can be within the accessible mass range, but due to the absence of color charge, may have eluded detection. This provides strong motivation for dedicated searches for electroweak SUSY particle production.

Depending on the mass spectrum, the charginos and neutralinos can have significant decay branching fractions to vector bosons V (W or Z), and Higgs bosons (H). Pair production of neutralinos and/or charginos can thus lead to HH, VH, and VV decay modes, yielding final states with at least one isolated lepton. Such final states can be easily selected with simple triggers and do not suffer from large QCD multijet backgrounds. Furthermore, the observation of a Higgs boson in a SUSY-like process would provide evidence that SUSY particles couple to the Higgs field, a necessary condition for SUSY to stabilize the Higgs boson mass. In this analysis we focus on chargino–neutralino production with the decay $\tilde{\chi}_1^\pm \to \mathrm{W}\tilde{\chi}_1^0$ and $\tilde{\chi}_2^0 \to \mathrm{H}\tilde{\chi}_1^0$ shown in Fig. 1. The W boson is required to decay leptonically. The lightest neutralino $\tilde{\chi}_1^0$ produced in decays of charginos and heavier neutralinos is considered to be the stable LSP which escapes detection. The process typically results in a signature with one lepton, two jets that originate in the $\mathrm{H} \to \mathrm{b\bar{b}}$ decay, and large missing transverse energy from the LSPs. The main background to this signature is top quark pair production decaying in a dilepton final state, with other smaller backgrounds including the production of W bosons with QCD jets. The backgrounds are estimated using Monte Carlo (MC) simulation and the predictions validated in data using control samples orthogonal to the signal selection.

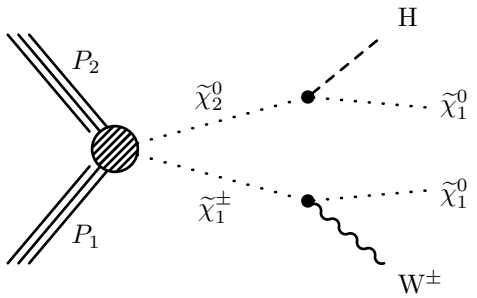

Figure 1: Feynman diagram of the SUSY simplified model targeted by this analysis: chargino-neutralino production with the chargino decaying to the W boson and the LSP, while the second neutralino decays to the Higgs boson and the LSP.

Results of searches for electroweak pair production of SUSY particles were previously reported by the ATLAS and CMS collaborations using datasets of 8 TeV proton-proton (pp) collisions [11–13]. These include different event topologies and final states. No excess above the SM expectations was observed and the results of those searches were used to place lower limits on the mass of pair produced charginos and neutralinos. Assuming degenerate $\tilde{\chi}_1^{\pm}$ and $\tilde{\chi}_2^0$, the searches probed their mass up to approximately 700 GeV. With the increase of the LHC collision energy from 8 to 13 TeV, and a significantly larger dataset, searches based on the 13 TeV data have the potential to quickly surpass the sensitivity of Run-1 analyses. This note presents the result of a search using a dataset corresponding to an integrated luminosity of 12.9 fb^{-1} of pp collisions collected at a center-of-mass energy of 13 TeV with the Compact Muon Solenoid (CMS) detector at the CERN LHC in 2016. The results are interpreted in a simplified model of supersymmetry [14–18] with chargino–neutralino production as depicted in Fig. 1.

2 Event samples, reconstruction, and selection

2.1 Object definition and pre-selection

Events are pre-selected using the requirements described in this section. They are then further classified into signal and control samples.

Event reconstruction is based on the particle-flow (PF) algorithm [19, 20], which combines information from the tracker, calorimeter, and muon systems to reconstruct and identify PF candidates, i.e. charged and neutral hadrons, photons, muons, and electrons. To select collision events we require at least one reconstructed vertex. If more than one vertex is present, the vertex with the largest sum of charge track p_T^2 value, referred to as the primary vertex, is taken. The missing transverse momentum vector, $\vec{p}_{\mathrm{T}}^{\,\mathrm{miss}}$, is defined as the negative vector sum of the momentum of all reconstructed particles projected onto the plane perpendicular to the LHC beams. Its magnitude is referred to as $E_{\mathrm{T}}^{\mathrm{miss}}$.

Data events are selected using triggers that require the presence of an isolated muon or electron with transverse momentum (p_{T}) thresholds of 22 GeV or 27 GeV, respectively. Muon events may also be accepted using a trigger that does not require isolation but instead requires $p_{\mathrm{T}} > 50$ GeV. The trigger efficiency, measured using a data sample of $\mathrm{Z}/\gamma^\star \to \ell\ell$ events, varies in the range $85-92\%$ ($75-95\%$) with an uncertainty of few percent for muons (electrons) and depends on the pseudorapidity η and p_{T} of the lepton.

Selected events are required to have exactly one lepton (muon or electron), with $p_{\mathrm{T}} > 25$ GeV and $|\eta| < 2.1$ ($p_{\mathrm{T}} > 30$ GeV and $|\eta| < 1.44$) for muons (electrons). Electrons in the forward region of the detector are not considered in this search due to the significant rate for a jet to be mis-identified as an electron in this region. Electron candidates are reconstructed starting from a cluster of energy deposits in the electromagnetic calorimeter. The cluster is then matched to a reconstructed track. The electron selection is based on the shower shape, track-cluster matching, and consistency between the cluster energy and the track momentum [21]. Muon candidates are reconstructed by performing a global fit that requires consistent hit patterns in the tracker and the muon system [22]. For both lepton flavors, the impact parameter with respect to the primary vertex is required to be less than 0.5 mm in the transverse plane and 1 mm along the beam direction.

Leptons are required to be isolated from other activity in the event. A measure of lepton isolation is the scalar p_{T} sum ($p_{\mathrm{T}}^{\mathrm{sum}}$) of all PF candidates not associated with the lepton within a cone of radius $\Delta R \equiv \sqrt{(\Delta\eta)^2 + (\Delta\phi)^2} = 0.3$, where $\Delta\eta$ and $\Delta\phi$ are the distances between the lepton

and the PF candidates at the primary vertex in η–ϕ space [23]. The average contribution of particles from additional pp interactions in the same or nearby bunch crossings (pileup) is estimated and subtracted from the $p_{\mathrm{T}}^{\mathrm{sum}}$ quantity. We require an isolation of $p_{\mathrm{T}}^{\mathrm{sum}} < 5$ GeV. Typical lepton identification and isolation efficiencies, measured in samples of $\mathrm{Z}/\gamma^{\star} \to \ell\ell$ events, are approximately 85–90% (80–85%) for muons (electrons), with variations depending on p_{T} and η. Small corrections are applied to simulation to match the efficiencies measured in data.

Particle-flow candidates are clustered to form jets using the anti-k_{T} clustering algorithm [24] with a distance parameter of 0.4, as implemented in the FASTJET package [25]. The pileup contribution to the jet energy is estimated on an event-by-event basis using the jet area method described in [26], and is subtracted from the overall jet p_{T}. Corrections are applied to the energy measurements of jets to account for non-uniform detector response and are propagated consistently as a correction to $\vec{p}_{\mathrm{T}}^{\,\mathrm{miss}}$. Jets overlapping with the selected lepton are not considered in the analysis.

Selected events are required to contain exactly two jets with $p_{\mathrm{T}} > 30$ GeV and $|\eta| < 2.4$. Both of these jets must be consistent with the decay of a heavy-flavor hadron, as identified using the medium operating point of the combined secondary vertex (CSVv2) tagging algorithm [27]. Such jets are refer to as b-tagged jets. The efficiency of this algorithm for b quark jets in the p_{T} range 30–400 GeV varies between approximately 60 and 65% for $|\eta| < 2.4$. The nominal misidentification rate for light-quark or gluon jets is approximately 1% [27] for the chosen working point.

Finally the $E_{\mathrm{T}}^{\mathrm{miss}}$ is required to exceed 100 GeV. Events with possible contributions from beam halo processes or anomalous noise in the calorimeter are rejected using dedicated filters [28].

The largest background in this search originates from $\mathrm{t\bar{t}}$ and tW production in dilepton final states, where one of the leptons is not reconstructed or identified. In order to reduce these backgrounds, we look for the presence of a second electron or muon with $p_{\mathrm{T}} > 5$ GeV and loose isolation requirements, and reject an event if such a lepton is found. Moreover, an event is rejected if, in addition to the selected lepton, it contains a reconstructed hadronic tau lepton with $p_{\mathrm{T}} > 20$ GeV, or an isolated track with $p_{\mathrm{T}} > 10$ GeV and opposite sign charge relative to the selected lepton. A track is considered isolated if the momentum sum in a cone of radius 0.3, determined using charged particle flow candidates consistent with the primary vertex, has an absolute value less than 6 GeV and a value relative to the track p_{T} less than 0.1.

2.2 Signal Region Definition

In the signal region we require the invariant mass of the two b-jets to be in the range $90 < M_{\mathrm{b\bar{b}}} < 150$ GeV, consistent with the Higgs boson mass within resolution. The $M_{\mathrm{b\bar{b}}}$ distribution for signal and background events is shown in Fig. 2 (top left).

To suppress single-lepton backgrounds originating from semi-leptonic $\mathrm{t\bar{t}}$, W+jets, and single top processes, a requirement on the transverse mass M_T of the lepton-neutrino system is imposed, where $M_T = \sqrt{2p_{\mathrm{T}}^{\ell}E_{\mathrm{T}}^{\mathrm{miss}}(1 - cos(\Delta\phi))}$ and $\Delta\phi$ is the angle between the transverse momentum of the lepton and $E_{\mathrm{T}}^{\mathrm{miss}}$. Background processes containing a single leptonically-decaying W boson have a kinematic endpoint $M_{\mathrm{T}} < M_{\mathrm{W}}$, modulo effects of the detector resolution and contributions from W bosons produced off mass shell. In this analysis we require $M_T > 150$ GeV, which significantly reduces single-lepton backgrounds as shown in Fig. 2 (bottom left).

In order to further suppress both semi-leptonic and dileptonic $\mathrm{t\bar{t}}$ background, we utilize the

contransverse mass variable, M_{CT} [29, 30]:

$$M_{CT}^2 = 2p_T^{b1}p_T^{b2}(1+\cos\Delta\phi_{bb}), \quad (1)$$

where p_T^{b1} and p_T^{b2} are transverse momenta of the two jets, and $\Delta\phi_{bb}$ is the azimuthal angle between the pair. As is shown in [29, 30], the variable has a kinematic endpoint at $(m^2(\delta) - m^2(\alpha))/m(\delta)$, where δ is the pair produced heavy particle and α is the invisible particle produced in the decay. In the case of $t\bar{t}$ events, the kinematic endpoint corresponds to the top quark mass, while signal events tend to have higher values of M_{CT}. This is shown in Fig. 2 (bottom right). We require $M_{CT} > 150$ GeV.

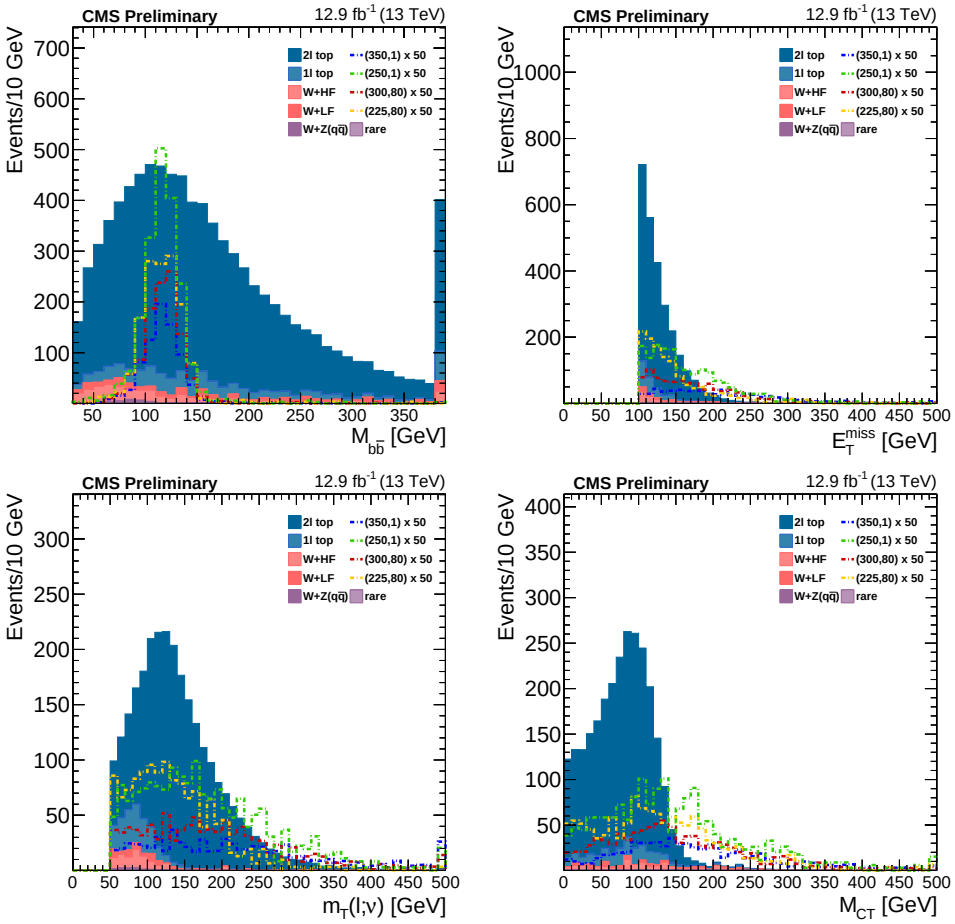

Figure 2: Distributions of $M_{b\bar{b}}$ (top left), E_T^{miss} (top right), M_T (bottom left), and M_{CT} (bottom right) for signal and background events in simulation after the preselection. The E_T^{miss}, M_T, and M_{CT} distributions are shown after the $90 < M_{b\bar{b}} < 150$ GeV requirement. Signal distributions are also overlaid as open histograms for various mass points. The legend entries for signal give the masses $(m_{\tilde{\chi}_1^\pm}, m_{\tilde{\chi}_1^0})$ and the amount by which the signal cross section has been scaled for display purposes.

2.3 Signal and background simulation

Background samples of $t\bar{t}$ W+jets and Z+jets events are generated using MADGRAPH V5 [31], while tW events are generated using POWHEG V2 [32–34]. A top quark mass of $m_t = 172.5$ GeV, and the NNPDF3.0 [35] parton distribution functions (PDF) are used in the event generation.

Single top s- and t-channel, as well as $\mathrm{t\bar{t}}$ production in association with a vector boson, are simulated using MADGRAPH_aMC@NLO 2.2 [36] generator. Depending on the final state, samples of diboson (WW, WZ, and ZZ) events are generated with either POWHEG V2 or MADGRAPH_aMC@NLO 2.2. Parton showering and fragmentation in all of these samples are performed using PYTHIA V8.1.

For both signal and background events, pileup interactions are simulated with PYTHIA and superimposed on the hard collisions, using a pileup multiplicity distribution that reflects the luminosity profile of the analyzed data. Standard model processes are simulated using a GEANT4-based model [37] of the CMS detector, while the simulation of new physics signals is performed using the CMS fast simulation package [38]. All simulated events are processed with the same chain of reconstruction programs used for collision data.

Small differences between the b tagging efficiencies measured in data and simulation [27] are corrected using data-to-simulation scale factors to adjust the b tagging probability in simulated events. A correction is also applied to account for differences between lepton selection efficiencies (trigger, reconstruction, identification, and isolation) in data and simulation.

3 Backgrounds

The backgrounds for this search are classified into six categories, based on the available control regions and strategies to estimate their contributions. The first and most important category is "Dilepton top quark," consisting mainly of $\mathrm{t\bar{t}} \to \ell\ell$ and also $t\mathrm{W} \to \ell\ell$ (where ℓ is a charged lepton). This category accounts for around 90% of the total background in the signal region. Next three categories include processes with a single leptonically-decaying W boson. These are all effectively suppressed by the requirement on M_{T} due to an endpoint at the W boson mass. The second category is "W + light jets," which here includes all flavors except b-jets (explicitly, udscg). The third category is from a W boson produced in association with b-jets, called W + HF for heavy flavor. The fourth category is WZ production, where the W boson decays leptonically and the Z boson decays to $\mathrm{b\bar{b}}$, referred to as $\mathrm{WZ} \to \ell\nu\mathrm{b\bar{b}}$. The fifth category is the "Single lepton top quark" background, consisting of $\mathrm{t\bar{t}} \to \ell +$ jets as well as single top quark t- and s-channel production. Finally, other standard model processes contribute a small amount to the expected yield in the signal region and are grouped together in the "Rare" category. This category includes the production of Z + jets, WW, WZ (except the decays described above), ZZ, triboson processes, $\mathrm{t\bar{t}W}$, $\mathrm{t\bar{t}Z}$, and $\mathrm{WH} \to \ell\nu\mathrm{b\bar{b}}$.

All of the background processes are modeled using MC simulation. Three data control regions are defined by inverting signal region selection requirements, to make them orthogonal to the signal region and reduce potential signal contamination. They are used to validate the modeling of the main backgrounds and assign associated systematic uncertainties. The control region selection requirements are summarized in Table 1. The expected signal contribution in any of the control regions is always less than 1% of the total standard model yields and typically much smaller.

The dilepton top quark background can be isolated by requiring two instead of one lepton, forming CR2ℓ. If all signal-like requirements are applied, the statistics are too low to validate the modeling of the dilepton top quark background. Therefore, CR2ℓ is used primarily to validate the modeling of $M_{\mathrm{b\bar{b}}}$.

The dijet mass range used to select the Higgs boson candidate is a natural requirement to invert. Inverting the $M_{\mathrm{b\bar{b}}}$ requirement yields CRM$\mathrm{b\bar{b}}$, which contains a mixture of all backgrounds in

Table 1: Control region selections compared with the signal region.

Cut	Signal Region	CR2ℓ	CR0b	CRMb$\bar{\text{b}}$
N(leptons)	$= 1$	$= 1$ or 2	$= 1$	$= 1$
Isolated track veto	✓	inverted if 1ℓ	✓	✓
Tau candidate veto	✓	inverted if 1ℓ	✓	✓
N(b-tags)	$= 2$	$= 2$	$= 0$	$= 2$
$M_{\text{b}\bar{\text{b}}}$	$\in$[90,150] GeV	-	$\in$[90,150] GeV	$\notin$[90,150] GeV
$E_{\text{T}}^{\text{miss}}$	> 100 GeV	> 100 GeV	> 100 GeV	> 100 GeV
M_{T}	> 150 GeV	> 50 GeV	> 150 GeV	> 150 GeV
M_{CT}	> 150 GeV	-	> 150 GeV	> 150 GeV

similar proportions to the signal region. Consequently, this control region is dominated by the dilepton top quark background and used to validate the modeling of these processes in the kinematic tails of $E_{\text{T}}^{\text{miss}}$, M_{T}, and M_{CT}. The systematic uncertainty in this background estimate is based on the level of agreement between data and MC.

The W + light jets background can be isolated by requiring exactly zero b-tagged jets instead of two, forming CR0b. This region is used to validate the modeling of the kinematic tails in $E_{\text{T}}^{\text{miss}}$, M_{T}, and M_{CT} for W+jets processes and assess a systematic uncertainty.

The background estimation and uncertainties are described in more detail in the following sections.

3.1 Dilepton top quark backgrounds

The dilepton top quark processes enter the signal region when the second lepton is not reconstructed or identified. The veto requirements on additional charged leptons or tracks reduce this background significantly. Due to the presence of two neutrinos, these backgrounds tend to have higher $E_{\text{T}}^{\text{miss}}$ than the single lepton backgrounds and do not have a bound at the W boson mass in M_{T}. The M_{CT} requirement significantly suppresses $\text{t}\bar{\text{t}} \to \ell\ell$ events, due to the end point feature near the top quark mass. The modeling of this background is validated in two steps. First, the modeling of $M_{\text{b}\bar{\text{b}}}$ is validated in CR2ℓ, which has a high purity for dilepton top quark events. Second, the modeling in the kinematic tails of $E_{\text{T}}^{\text{miss}}$, M_{T}, and M_{CT} is validated in CRMb$\bar{\text{b}}$ and a systematic uncertainty assessed based on the level of agreement between data and MC. Figure 3 (left) shows the distribution of $M_{\text{b}\bar{\text{b}}}$ sideband after preselection requirements. The shape of $M_{\text{b}\bar{\text{b}}}$ agrees well between data and MC.

Figure 3 (right) shows the distribution of $M_{\text{b}\bar{\text{b}}}$ in CRMb$\bar{\text{b}}$ after the preselection requirements, where already the dilepton top quark background is dominant. Good shape agreement is observed here as well. Table 2 then gives the predicted and observed yields in CRMb$\bar{\text{b}}$ including the signal region selections on $E_{\text{T}}^{\text{miss}}$, M_{T}, and M_{CT}. After the predictions for the other background components are subtracted, good agreement is observed between the data yields and the prediction of the number of dilepton top quark events. We assign a systematic uncertainty of 20% on the prediction of dilepton top quark in the signal region based on the statistical precision of this comparison. This accounts for any effects that could impact the modeling of this background in simulation, including generator factorization and renormalization scales, PDF, jet energy scale, as well as b-tagging, lepton identification and isolation, and trigger efficiencies.

3.2 W boson backgrounds

The requirement of $M_{\text{T}} > 150$ GeV effectively suppresses the contribution from W+jets events, as they typically have an endpoint at the W boson mass. However, events from W+jets can still enter the M_{T} tail due to off-shell W production or $E_{\text{T}}^{\text{miss}}$ resolution effects. The control region

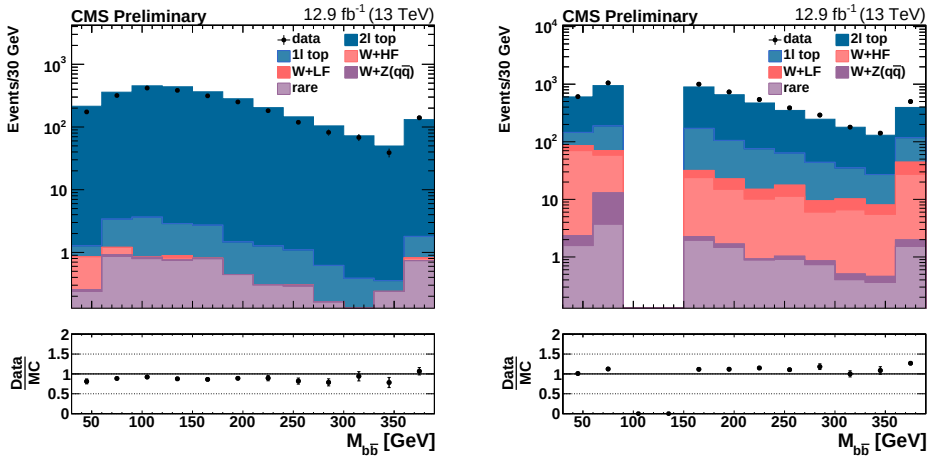

Figure 3: (Left) Distribution of $M_{b\bar{b}}$ in CR2ℓ after preselection requirements, comparing data to MC simulation. (Right) Distribution of $M_{b\bar{b}}$ in CRMb$\bar{b}$ after preselection requirements.

Table 2: Predicted and observed yields for CRMb$\bar{b}$ after the signal region requirements on $E_{\mathrm{T}}^{\mathrm{miss}}$, M_{T}, and M_{CT}. The observed data yield is compared to the MC prediction for the dilepton top quark background after subtracting the predictions for the other (non-dilepton top quark) backgrounds. The uncertainties shown are statistical only, and the uncertainty on the ratio includes the statistical uncertainty on the data and MC samples.

data	29
Dilepton top quark	28.6 ± 2.0
W + light jets	0.3 ± 0.1
W + HF	1.5 ± 0.6
WZ $\to \ell\nu b\bar{b}$	0.00 ± 0.04
Single lepton top quark	0.9 ± 0.5
Rare	0.8 ± 0.2
All MC	32.0 ± 2.1
data-others	25.6 ± 5.4
data-others/MC(Dilepton top quark)	0.90 ± 0.20

CR0b has high purity for W + light jets and is therefore used to validate the modeling of W+jets in the tails of the kinematic variables, most importantly for M_{T}.

Table 3 shows the yields in CR0b with all the signal kinematic requirements applied, including $M_{\mathrm{T}} > 150$ GeV. We see that the prediction in this kinematic region is lower than the data by an amount slightly exceeding the statistical uncertainty. From this test, we take the level of agreement as correction factor of 1.17 for W+jets, and assign the full correction of 17% as a systematic uncertainty on the modeling of W+jets. This procedure directly tests the background from W+jets in the kinematic phase space of the signal region, including the effects from generator factorization and renormalization scales, PDF, jet energy scale, as well as lepton identification, isolation, and trigger efficiency. We assign additional uncertainties to each of the W+jets background categories as described below to account for other potential effects not covered by this comparison.

For W + light jets backgrounds, we evaluate the uncertainty due to the b-tagging requirements by varying the b-tagging efficiencies within their measured uncertainties. The uncertainty on the yield in the signal region amounts to 1%.

Table 3: Yields for CR0b, after all signal region requirements, including $M_{\mathrm{T}} > 150$ GeV. The observed data yield is compared to the W + light jets MC prediction after subtracting the prediction for the other (non W + light jets) backgrounds from the data yield. The uncertainties shown are statistical only, and the uncertainty on the ratio includes the statistical uncertainty on the data and MC samples.

data	210
Dilepton top quark	43.7 ± 2.4
W + light jets	110.1 ± 6.5
W + HF	1.6 ± 0.8
WZ $\to \ell\nu\mathrm{b\bar{b}}$	1.1 ± 0.2
Single lepton top quark	3.7 ± 0.9
Rare	30.9 ± 1.7
All MC	191.0 ± 7.2
data-others	129.0 ± 14.8
data-others/MC(W + light jets)	1.17 ± 0.15

For W + HF backgrounds, the effects contributing to the kinematic tails will be similar to W + light jets. The tail of M_{T} receives contributions from off-shell W production, $E_{\mathrm{T}}^{\mathrm{miss}}$ resolution effects, and additional neutrinos from semi-leptonic decays within the b-jets. For this last contribution, we expect this background to be well modeled in MC as it involves true $E_{\mathrm{T}}^{\mathrm{miss}}$, plus the kinematics of the jets in W+jets are seen to be well reproduced by MC in CR0b. Thus we do not apply any additional correction or uncertainty for kinematic tail modeling beyond the one derived above in CR0b.

The most uncertain aspect of the prediction for W + HF is the cross section relative to W + light jets. We follow the recipe applied in Ref. [39] and assign a 50% uncertainty to the normalization of this background. This uncertainty is validated by comparing data to simulation in a data control region dominated by W+jets, requiring presence of one or two jets and $60 < M_{\mathrm{T}} < 120$ GeV. The uncertainty is seen to conservatively cover any differences between data and simulation as a function of the number of b-tags. We also evaluate the uncertainty on this prediction due to the uncertainty on b-tagging efficiency, and we find the impact to be 5%.

For the WZ $\to \ell\nu\mathrm{b\bar{b}}$ background, we expect again the same effects to contribute to the tail of M_{T}, and we apply the same tail modeling systematic uncertainty derived from CR0b above. We apply an uncertainty of 12% to the normalization of WZ $\to \ell\nu\mathrm{b\bar{b}}$, based on the CMS cross section measurement of inclusive WZ production at 13 TeV [40]. The other unique aspect of WZ $\to \ell\nu\mathrm{b\bar{b}}$ is that $M_{\mathrm{b\bar{b}}}$ peaks at the Z boson mass, at the lower edge of the $M_{\mathrm{b\bar{b}}}$ selection used in this analysis. Uncertainties in the jet energy scale can therefore strongly impact the prediction of this background. We vary the jet energy scale within its measured uncertainty and find an impact of 27% on this background prediction, although the absolute magnitude of this background remains very small in the signal region. We also evaluate the uncertainty on this prediction due to the uncertainty on b-tagging efficiency and find the impact to be 2%.

3.3 Other backgrounds

The single lepton top quark backgrounds are highly suppressed by several of the selections applied in this analysis. Since these have exactly one W boson, the M_{T} requirement is an effective handle against them. Requiring exactly two jets also suppresses $\mathrm{t\bar{t}} \to \ell$ + jets, which typically has four jets in the final state. As a result, this background comprises less than 5% of

Table 4: Expected and observed yields in the signal region. The expected yields for some example signal points are also given. The uncertainties include both statistical and systematic sources.

data	8
Dilepton top quark	8.9 ± 2.0
W + light jets	0.01 ± 0.01
W + HF	0.7 ± 0.5
WZ $\to \ell\nu b\bar{b}$	0.03 ± 0.03
Single lepton top quark	0.3 ± 0.3
Rare	0.3 ± 0.2
Total bkg	10.3 ± 2.1
$(m_{\tilde{\chi}_1^\pm}, m_{\tilde{\chi}_1^0})$ (225,75)	1.7 ± 0.3
$(m_{\tilde{\chi}_1^\pm}, m_{\tilde{\chi}_1^0})$ (250,1)	5.6 ± 0.8
$(m_{\tilde{\chi}_1^\pm}, m_{\tilde{\chi}_1^0})$ (300,75)	4.1 ± 0.5
$(m_{\tilde{\chi}_1^\pm}, m_{\tilde{\chi}_1^0})$ (350,1)	4.1 ± 0.4

the expected standard model prediction in the signal region.

Isolating the single lepton top quark backgrounds in a region kinematically similar to the signal region is difficult. The main source of uncertainty in the prediction of the single lepton top quark backgrounds is the modeling of the $E_{\mathrm{T}}^{\mathrm{miss}}$ resolution, since a small difference in data and MC simulation could translate into a large number of additional events passing the M_{T} requirement. From CR0b, we observe that M_{T} is well modeled in MC.

Additional studies comparing $E_{\mathrm{T}}^{\mathrm{miss}}$ resolution in data and simulation are performed using γ + jets events. The resolution in data is found to be up to 20% worse than in simulation, leading to higher single lepton top quark yields than expected from simulation. However, when propagated to the size of the total background, the effect is negligible. Based on this study, and the fact that this background gives a small contribution to the total expectation, we assign a uncertainty of 100% on this contribution.

The "rare" backgrounds also contribute less than 5% of the expected yield in the signal region. We apply a conservative uncertainty of 100% on the yields of the processes.

4 Results

Figure 4 shows the distribution of $M_{\mathrm{b\bar{b}}}$ for data and the MC prediction after all other signal region requirements. The data agree with the prediction in both the signal region and in CRMb$\bar{\mathrm{b}}$, defined as the region outside the signal range in $M_{\mathrm{b\bar{b}}}$ and discussed in Section 3.1. Table 4 shows the expected background yields in the signal region compared to the observation. We observe eight events in data with an SM expectation of 10.3 ± 2.1.

5 Interpretation

The results of this analysis are interpreted in the context of the simplified SUSY model depicted in Fig. 1, $\tilde{\chi}_1^\pm \tilde{\chi}_2^0 \to \mathrm{WH}\tilde{\chi}_1^0 \tilde{\chi}_1^0$. The $\tilde{\chi}_1^\pm$ and $\tilde{\chi}_2^0$ particles are assumed to be degenerate in mass, and the branching fractions for the decays listed above are assumed to be 100%. The W and Higgs

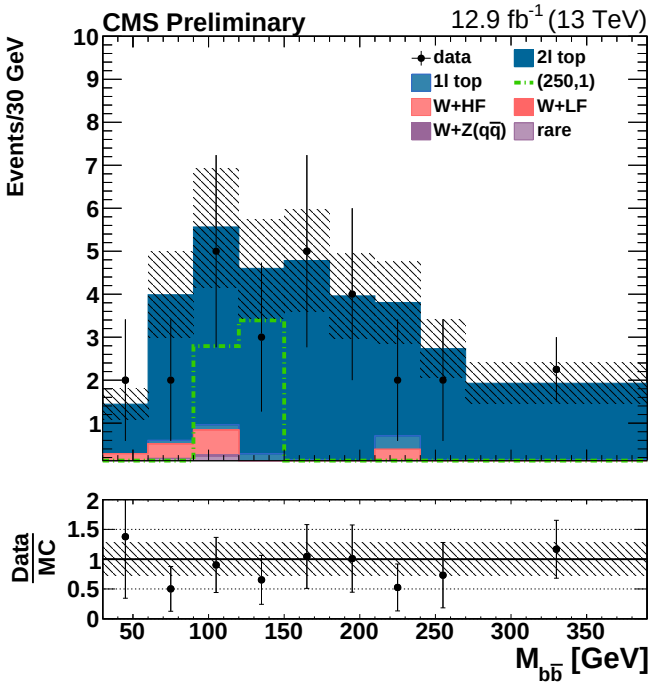

Figure 4: Distribution of $M_{b\bar{b}}$ after all signal region kinematic requirements. The signal region corresponds to the bins with $90 < M_{b\bar{b}} < 150$ GeV. The hatched band shows the total uncertainty on the background prediction, including statistical and systematic components. The signal distribution for a reference mass point is overlaid as an open histogram, and the legend entry for signal gives the masses $(m_{\tilde{\chi}_1^\pm}, m_{\tilde{\chi}_1^0})$.

bosons decay according to their standard model branching fractions. Upper limits on the new-physics cross sections are derived from the yields in the one signal region using a modified frequentist approach, employing the CL_s method and an asymptotic formulation [41–44].

The systematic uncertainties considered on the signal yield are summarized in Table 5 along with their typical values. The signal points with the largest uncertainties are those with $\Delta m = m_{\tilde{\chi}_1^\pm} - m_{\tilde{\chi}_1^0} \simeq m_H$. Kinematic properties of these signal events are most similar to the standard model backgrounds and the acceptance is thus smaller than for points with larger Δm values. For these points with compressed mass splittings, the largest uncertainties in the signal yields arise from the jet energy scale (up to 27%), E_T^{miss} resolution in fast simulation (up to 50%), and limited MC statistics (up to 40%). For points with larger Δm values, the largest uncertainties come again from the E_T^{miss} resolution in fast simulation (typically 5–10%) and from the uncertainty in the integrated luminosity (6.2%). Other experimental and theoretical uncertainties are also considered and lead to smaller changes in the expected yields, including generator renormalization and factorization scales, b-tagging efficiency, lepton reconstruction, identification, and isolation efficiency, and trigger efficiency.

Figure 5 then shows the expected and observed 95% confidence level (CL) exclusion limits on the cross section for $\tilde{\chi}_1^\pm \tilde{\chi}_2^0 \to WH\tilde{\chi}_1^0\tilde{\chi}_1^0$ as a function of chargino mass assuming an LSP with a mass of 1 GeV. The next-to-leading-order (NLO) theoretical cross section for production of $\tilde{\chi}_1^\pm \tilde{\chi}_2^0$ is also shown, assuming these are pure wino states [45, 46].

Table 5: Sources of systematic uncertainty on the estimated signal yield along with their typical values. The ranges represent variation across the signal masses probed.

Source	Typical Values
Integrated luminosity	6.2%
MC statistics	3–40%
Renormalization and factorization scales	1–3%
B-tagging efficiency	2–3%
Lepton efficiency	2–5%
Trigger efficiency	1–5%
Jet energy scale	1–27%
Fastsim $E_{\mathrm{T}}^{\mathrm{miss}}$ resolution	5–50%

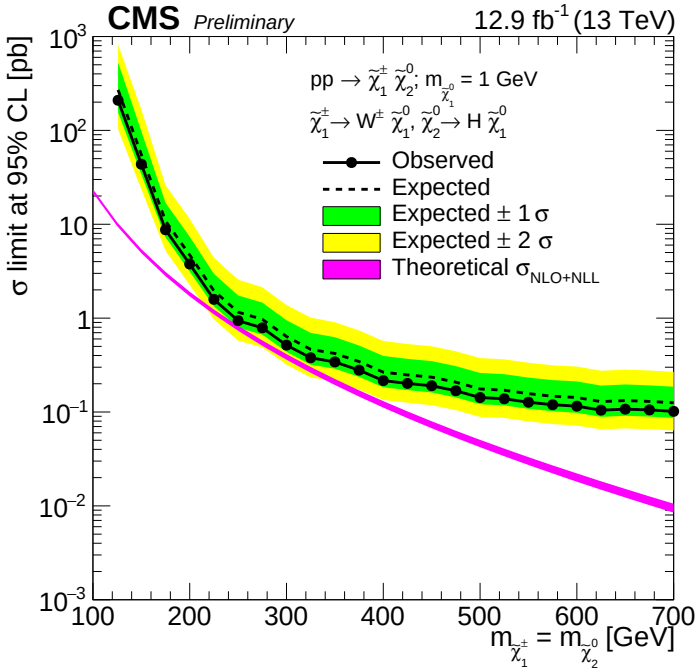

Figure 5: Expected and observed cross section limits at the 95% CL as a function of the chargino mass, where the LSP is assumed to have a mass of 1 GeV. The NLO theoretical cross section for production of $\tilde{\chi}_1^{\pm}\tilde{\chi}_2^0$ is also shown, assuming these are pure wino states.

6 Conclusions

A search was performed for beyond the standard model physics in events with a leptonically-decaying W boson, a Higgs boson decaying to a $\mathrm{b\bar{b}}$ pair, and $E_{\mathrm{T}}^{\mathrm{miss}}$, using 12.9 fb^{-1} of data recorded by CMS in 2016 at $\sqrt{s} = 13$ TeV. The observed data are in agreement with the standard model expectation. The results were used to set cross section limits on chargino-neutralino production in a simplified SUSY model with the decays $\tilde{\chi}_1^{\pm} \to \mathrm{W}\tilde{\chi}_1^0$ and $\tilde{\chi}_2^0 \to \mathrm{H}\tilde{\chi}_1^0$.

References

[1] P. Ramond, "Dual theory for free fermions", *Phys. Rev. D* **3** (1971) 2415, doi:10.1103/PhysRevD.3.2415.

[2] Y. A. Golfand and E. P. Likhtman, "Extension of the algebra of Poincaré group generators and violation of P invariance", *JETP Lett.* **13** (1971) 323.

[3] A. Neveu and J. H. Schwarz, "Factorizable dual model of pions", *Nucl. Phys. B* **31** (1971) 86, doi:10.1016/0550-3213(71)90448-2.

[4] D. V. Volkov and V. P. Akulov, "Possible universal neutrino interaction", *JETP Lett.* **16** (1972) 438.

[5] J. Wess and B. Zumino, "A Lagrangian model invariant under supergauge transformations", *Phys. Lett. B* **49** (1974) 52, doi:10.1016/0370-2693(74)90578-4.

[6] J. Wess and B. Zumino, "Supergauge transformations in four dimensions", *Nucl. Phys. B* **70** (1974) 39, doi:10.1016/0550-3213(74)90355-1.

[7] P. Fayet, "Supergauge invariant extension of the Higgs mechanism and a model for the electron and its neutrino", *Nucl. Phys. B* **90** (1975) 104, doi:10.1016/0550-3213(75)90636-7.

[8] H. P. Nilles, "Supersymmetry, supergravity and particle physics", *Phys. Rep.* **110** (1984) 1, doi:10.1016/0370-1573(84)90008-5.

[9] C. Boehm et al., "Light Scalar Top Quarks and Supersymmetric Dark Matter", *Phys. Rev. D* **62** (2000) 035012, doi:10.1103/PhysRevD.62.035012, arXiv:hep-ph/9911496.

[10] C. Balázs et al., "Dark Matter, Light Stops and Electroweak Baryogenesis", *Phys. Rev. D* **70** (2004) 015007, doi:10.1103/PhysRevD.70.015007, arXiv:hep-ph/403224.

[11] CMS Collaboration, "Searches for electroweak neutralino and chargino production in channels with Higgs, Z, and W bosons in pp collisions at 8 TeV", *Phys. Rev. D* **90** (2014), no. 9, 092007, doi:10.1103/PhysRevD.90.092007, arXiv:1409.3168.

[12] CMS Collaboration, "Searches for electroweak production of charginos, neutralinos, and sleptons decaying to leptons and W, Z, and Higgs bosons in pp collisions at 8 TeV", *Eur. Phys. J. C* **74** (2014), no. 9, 3036, doi:10.1140/epjc/s10052-014-3036-7, arXiv:1405.7570.

[13] ATLAS Collaboration, "Search for the electroweak production of supersymmetric particles in $\sqrt{s}$=8 TeV pp collisions with the ATLAS detector", *Phys. Rev. D* **93** (2016), no. 5, 052002, doi:10.1103/PhysRevD.93.052002, arXiv:1509.07152.

[14] N. Arkani-Hamed et al., "MARMOSET: The path from LHC data to the new standard model via on-shell effective theories", (2007). arXiv:hep-ph/0703088.

[15] J. Alwall, P. Schuster, and N. Toro, "Simplified models for a first characterization of new physics at the LHC", *Phys. Rev. D* **79** (2009) 075020, doi:10.1103/PhysRevD.79.075020, arXiv:0810.3921.

[16] J. Alwall, M.-P. Le, M. Lisanti, and J. G. Wacker, "Model-independent jets plus missing energy searches", *Phys. Rev. D* **79** (2009) 015005, doi:10.1103/PhysRevD.79.015005, arXiv:0809.3264.

[17] D. Alves et al., "Simplified models for LHC new physics searches", *J. Phys. G* **39** (2012) 105005, doi:10.1088/0954-3899/39/10/105005, arXiv:1105.2838.

[18] CMS Collaboration, "Interpretation of searches for supersymmetry with simplified models", *Phys. Rev. D* **88** (2013) 052017, doi:10.1103/PhysRevD.88.052017, arXiv:1301.2175.

[19] CMS Collaboration, "Particle-flow event reconstruction in CMS and performance for jets, taus, and $E_{\mathrm{T}}^{\mathrm{miss}}$", CMS Physics Analysis Summary CMS-PAS-PFT-09-001, 2009.

[20] CMS Collaboration, "Commissioning of the particle-flow event with the first LHC collisions recorded in the CMS detector", CMS Physics Analysis Summary CMS-PAS-PFT-10-001, 2010.

[21] CMS Collaboration, "Performance of electron reconstruction and selection with the CMS detector in proton-proton collisions at $\sqrt{s} = 8$ TeV", *JINST* **10** (2015) P06005, doi:10.1088/1748-0221/10/06/P06005, arXiv:1502.02701.

[22] CMS Collaboration, "Performance of CMS muon reconstruction in pp collision events at $\sqrt{s} = 7$ TeV", *JINST* **7** (2012) P10002, doi:10.1088/1748-0221/7/10/P10002, arXiv:1206.4071.

[23] CMS Collaboration, "Description and performance of track and primary-vertex reconstruction with the CMS tracker", *JINST* **9** (2014) P10009, doi:10.1088/1748-0221/9/10/P10009, arXiv:1405.6569.

[24] M. Cacciari, G. P. Salam, and G. Soyez, "The anti-k_{T} jet clustering algorithm", *JHEP* **04** (2008) 063, doi:10.1088/1126-6708/2008/04/063, arXiv:0802.1189.

[25] M. Cacciari, G. P. Salam, and G. Soyez, "FastJet User Manual", *Eur. Phys. J. C* **72** (2012) 1896, doi:10.1140/epjc/s10052-012-1896-2, arXiv:1111.6097.

[26] M. Cacciari and G. P. Salam, "Pileup subtraction using jet areas", *Phys. Lett. B* **659** (2008) 119, doi:10.1016/j.physletb.2007.09.077, arXiv:0707.1378.

[27] CMS Collaboration, "Identification of b-quark jets with the CMS experiment", *JINST* **8** (2013) P04013, doi:10.1088/1748-0221/8/04/P04013, arXiv:1211.4462.

[28] CMS Collaboration, "Missing transverse energy performance of the CMS detector", *JINST* **6** (2011) P09001, doi:10.1088/1748-0221/6/09/P09001, arXiv:1106.5048.

[29] D. R. Tovey, "On measuring the masses of pair-produced semi-invisibly decaying particles at hadron colliders", *JHEP* **04** (2008) 034, doi:10.1088/1126-6708/2008/04/034, arXiv:0802.2879.

[30] G. Polesello and D. R. Tovey, "Supersymmetric particle mass measurement with the boost-corrected contransverse mass", *JHEP* **03** (2010) 030, doi:10.1007/JHEP03(2010)030, arXiv:0910.0174.

[31] J. Alwall et al., "MADGRAPH 5: going beyond", *JHEP* **06** (2011) 128, doi:10.1007/JHEP06(2011)128, arXiv:1106.0522.

[32] P. Nason, "A new method for combining NLO QCD with shower Monte Carlo algorithms", *JHEP* **11** (2004) 040, doi:10.1088/1126-6708/2004/11/040, arXiv:hep-ph/0409146.

[33] S. Frixione, P. Nason, and C. Oleari, "Matching NLO QCD computations with parton shower simulations: the POWHEG method", *JHEP* **11** (2007) 070, doi:10.1088/1126-6708/2007/11/070, arXiv:0709.2092.

[34] S. Alioli, P. Nason, C. Oleari, and E. Re, "A general framework for implementing NLO calculations in shower Monte Carlo programs: the POWHEG BOX", *JHEP* **06** (2010) 043, doi:10.1007/JHEP06(2010)043, arXiv:1002.2581.

[35] NNPDF Collaboration, "Parton distributions for the LHC Run II", *JHEP* **04** (2015) 040, doi:10.1007/JHEP04(2015)040, arXiv:1410.8849.

[36] J. Alwall et al., "The automated computation of tree-level and next-to-leading order differential cross sections, and their matching to parton shower simulations", *JHEP* **07** (2014) 079, doi:10.1007/JHEP07(2014)079, arXiv:1405.0301.

[37] GEANT4 Collaboration, "GEANT4 — a simulation toolkit", *Nucl. Instrum. Meth. A* **506** (2003) 250, doi:10.1016/S0168-9002(03)01368-8.

[38] S. Abdullin et al., "The fast simulation of the CMS detector at LHC", *J. Phys. Conf. Ser.* **331** (2011) 032049, doi:10.1088/1742-6596/331/3/032049.

[39] CMS Collaboration, "Search for direct top squark pair production in the single lepton final state at $\sqrt{s} = 13$ TeV", Technical Report CMS-PAS-SUS-16-002, CERN, Geneva, 2016.

[40] CMS Collaboration, "Measurement of the WZ production cross section in pp collisions at sqrt(s) = 13 TeV", Technical Report CMS-PAS-SMP-16-002, CERN, Geneva, 2016.

[41] A. L. Read, "Presentation of search results: The CL_s technique", *J. Phys. G* **28** (2002) 2693, doi:10.1088/0954-3899/28/10/313.

[42] T. Junk, "Confidence level computation for combining searches with small statistics", *Nucl. Instrum. Meth. A* **434** (1999) 435, doi:10.1016/S0168-9002(99)00498-2, arXiv:hep-ex/9902006.

[43] G. Cowan, K. Cranmer, E. Gross, and O. Vitells, "Asymptotic formulae for likelihood-based tests of new physics", *Eur. Phys. J. C* **71** (2011) 1554, doi:10.1140/epjc/s10052-011-1554-0, arXiv:1007.1727.

[44] ATLAS and CMS Collaborations, "Procedure for the LHC Higgs boson search combination in summer 2011", Technical Report ATL-PHYS-PUB-2011-011, CMS-NOTE-2011-005, 2011.

[45] B. Fuks, M. Klasen, D. R. Lamprea, and M. Rothering, "Gaugino production in proton-proton collisions at a center-of-mass energy of 8 TeV", *JHEP* **10** (2012) 081, doi:10.1007/JHEP10(2012)081, arXiv:1207.2159.

[46] B. Fuks, M. Klasen, D. R. Lamprea, and M. Rothering, "Precision predictions for electroweak superpartner production at hadron colliders with RESUMMINO", *Eur. Phys. J. C* **73** (2013) 2480, doi:10.1140/epjc/s10052-013-2480-0, arXiv:1304.0790.